Carrier thermal escape in families of InAs/InP self-assembled quantum dots

Guillaume Gélinas, Ali Lanacer, and Richard Leonelli*
Département de Physique and Regroupement Québécois sur les Matériaux de Pointe (RQMP), Université de Montréal, Case Postale 6128, Succursale Centre-ville, Montréal, Québec, Canada H3C 3J7

Remo A. Masut
Département de Génie Physique and Regroupement Québécois sur les matériaux de pointe (RQMP), École Polytechnique, Case Postale 6079, Succursale Centre-ville, Montréal, Québec, Canada H3C 3A7

Philip J. Poole
Institute for Microstructural Sciences, National Research Council of Canada, 1200 Montreal Road, Ottawa, Ontario, Canada K1A 0R6
(Received 15 October 2009; revised manuscript received 24 May 2010; published 18 June 2010)

The temperature evolution of the photoluminescence spectra of two samples of single-layer InAs/InP (001) self-assembled quantum dots is measured from 10 to 300 K. To understand the thermal quenching of their multimodal emission, we develop a coupled rate-equation model that includes the effect of carrier thermal escape from a quantum dot to the wetting layer and to the InP matrix, followed by transport, recapture or nonradiative recombination. Our model reproduces the temperature dependence of the emission of each family of quantum dots with a single set of parameters. We find that the main escape mechanism of the carriers confined in the quantum dots is through thermal emission to the wetting layer. The activation energy for this process is found to be close to one half the energy difference between that of a given family of quantum dots and that of the wetting layer as measured by photoluminescence excitation experiments. This indicates that electron and holes exit the InAs quantum dots as correlated pairs.

DOI: 10.1103/PhysRevB.81.235426 PACS number(s): 78.67.Hc, 78.55.Cr

I. INTRODUCTION

Quantum dots (QDs) are designable mesoscopic atomic assemblies whose effective electronic density of states is δ functionlike.[1] One of the most studied systems is self-assembled QDs grown in the Stransky-Krastanow mode. It has been demonstrated that self-assembled QDs can find applications in fields ranging from nano-optoelectronics[2] to quantum computing.[3] Understanding the processes that result in the thermal quenching of the photoluminescence (PL) of QDs is thus important not only on fundamental grounds but also for the realization of efficient devices operating at room temperature.

In the case of InAs/GaAs QDs, it is now well established that the two mechanisms that control the populations of electron-hole pairs in the ground state of QDs are their radiative recombination and their escape to higher-lying energy states. Thermal quenching then results from nonradiative recombination processes that occur in one or several of those higher-energy states.[4–16] Even though both measurements and theoretical modeling appear straightforward, there remains to this day significant differences and apparent contradictions in the interpretation of the results published by different groups over the last decade.

Two important questions remain unanswered. First, the identification of the higher-energy states that contain nonradiative centers. Potential candidates are (i) the so-called wetting layer (WL), which is a few monolayer (ML) thick InAs pseudomorphic quantum well (QW) always present in the Stranski-Krastanow growth mode; (ii) the matrix in which the QDs are inserted, either GaAs or a confining QW; (iii) defects or impurities in the matrix; or (iv) QD excited states. Second, it is still not clear whether the confined electrons and holes escape a QD as a single quasiparticle (exciton) or as independent carriers. The nature of the escape mechanism can be revealed indirectly by the ratio

$$\nu = E_i^a/\Delta E_i, \tag{1}$$

where E_i^a is the measured thermal activation energy and ΔE_i is the optical gap between the emission from the higher-energy state i and that of the QDs. In the case of exciton escape, $E_i^a = \Delta E_i$ and $\nu = 1$. If single carrier escape dominates, E_i^a corresponds to the confinement energy of the less confined carrier and $\nu < 1/2$. Yang *et al.*[4] pointed to another possibility: that of a correlated *e-h* pair escape. No detailed correlation mechanism was proposed but it could arise, for example, if the escape of one of the carriers changes the potential landscape enough to induce dynamically the escape of the second one. As electrons and holes would then be, in average, emitted in pairs, their concentrations would be equal and thus determined by only half the optical gap energy ΔE_i. It follows that, in the case of a correlated pair escape, $\nu = 1/2$.

Carrier capture and recombination in QDs are random processes that require a master equation formalism in order to properly describe QD excited state dynamics.[17–20] However, under continuous-wave, low excitation conditions where the average number of electron-hole pairs per QD is much smaller than one, the predictions of more conventional and simple rate-equation models remain valid. Further, QD-size fluctuations result in a distribution of their quantized energies and hence to a distribution of activation energies. As temperature is increased, redistribution of the carrier population occurs toward the low-energy tail of the QD energy distribution.[4–6,9,11] When the full width at half maximum (FWHM) of the emission of the ensemble of QDs is much smaller than any expected activation energy, the QD energy

 ©2010 The American Physical Society

distribution is often represented by a δ function. The solution of the thermal rate equations in steady state for the ensemble PL intensity I then gives

$$I(T) = I_0\left(1 + \sum_{i=1}^{m} A_i e^{-E_i^a/kT}\right)^{-1}, \quad (2)$$

where m is the number of high-energy states involved and E_i^a is the activation energy for the transfer from QD to state i.[12] Using this approach, Heitz *et al.*[5] pointed to transitions from the ground-state exciton to QD excited states and to the WL while Le Ru *et al.*[7] identified the GaAs matrix as the dominant recombination state and obtained $\nu=1$. Using samples where the QDs were imbedded in an InGaAs QW, Torchysnka *et al.*[12,14] found several activation energies that corresponded well to transitions from QDs to QW and from QW to the GaAs matrix, assuming $\nu=1$. Schulz *et al.* reported on InP QDs embedded in $(Al_xGa_{1-x})_{0.51}In_{0.49}P$ with a bimodal height distribution. They found that the activation energy of the smaller dots corresponded to exciton escape while that of the larger dots was compatible with correlated pair escape.[15] Seravalli *et al.* examined samples where the QDs were inserted in $In_xGa_{1-x}As$ and $In_{1-y}Al_yAs$ confining layers. They found two dominant activation energies that corresponded to exciton transitions from QDs to an unidentified low-energy defect and transitions from QDs to the WL.[16]

More information is available if the internal population redistribution is also measured and modeled. In that case, the rate equations must take into account the QD energy distribution. Yang *et al.*[4] analyzed the PL decay times within the QD emission band with a model that only included the WL as the high-energy state. They found good agreement with experimental data with $\nu \approx 1/2$. However, the validity their rate-equation model under pulsed excitation conditions is questionable.[19] Sanguinetti *et al.*[6] developed a model that included exciton transitions from QDs to WL and WL to the GaAs matrix. It reproduced well the QD PL integrated intensity, FWHM, and peak energy as a function of temperature. Akiba *et al.*[8] studied InAs QDs in GaAs layers with a trimodal height distribution. Their model, which assumed correlated pair escape, reproduced qualitatively the PL integrated intensity of the individual QD families as well as that of the WL. Dawson *et al.*[9,11] included in their model independent distributions of electrons and holes but they only considered transitions from QDs to the GaAs matrix. They found that the PL integrated intensity, FWHM, and peak energy was best fitted by uncorrelated carrier escape.

The reason for these discrepancies is unclear. One might point out different escape mechanisms in different samples, insufficient information provided by a single QD emission band, or differences in the theoretical models and/or assumptions underlying their treatment. On the other hand, little work of a similar nature has been carried out on equivalent QDs grown on materials systems with an energy spectrum quantitatively different from that of InAs/GaAs. In order to solve some of the problems mentioned above, we present a study of the thermal quenching from two samples that contain a single layer of InAs QDs embedded in an InP matrix. Their PL spectra show several well-resolved emission bands, extending from 0.75 to 1.1 eV, that can be associated with families of QDs that differ in height by 1 ML,[21–28] while their PL excitation (PLE) spectra reveal absorption edges that we associate with QD excited states and WL resonances. The evolution with temperature of the multimodal PL of our samples imposes stringent constraints on a model based on coupled rate equations as it should reproduce the thermal behavior of many peaks with the same set of parameters.

II. EXPERIMENTAL PROCEDURES

Sample A was grown by low-pressure metal-organic vapor-phase epitaxy on (001) InP Fe-doped semi-insulating substrates at a reactor pressure of 160 torr. Trimethylindium (TMI), tertiarybutylarsine (TBA), and tertiarybutylphosphine (TBP) were used as precursors and Pd-purified H_2 as the carrier gas. The flow rates of TMI and TBA were kept at 0.05 and 0.95 μmol s^{-1} and the TBP flow rate was 3.5 μmol s^{-1}. After the growth at 600 °C of a 100 nm InP buffer layer, the temperature was lowered to 500 °C during 90 s while still growing InP. 2.4 InAs MLs, sandwiched between two 20-ML-thick InP layers, were then deposited at 500 °C. The temperature was raised back to 600 °C and the growth terminated by the deposition of a 30 nm InP cap layer. The growth interruption sequence used to switch from InP to InAs and back is described in Ref. 29. In particular, a 4 s growth interruption was applied after InAs deposition.

Sample B was grown on (001) InP substrates by chemical-beam epitaxy from TMI, arsine (AsH_3), and phosphine (PH_3). AsH_3 and PH_3 were cracked at 850 °C in a fast switching high-temperature injector to produce predominantly As_2 and P_2. After desorption of the surface oxide, the growth was initiated with an InP buffer layer. Then, TMI and As_2 were injected simultaneously into the chamber to grow about 2.2 MLs of InAs layer at 515 °C. This was followed by a 30 s growth interruption under an overpressure of As_2 to allow the QDs to form. The QDs were then capped with InP. Further information on the growth procedure can be found in Ref. 28.

The PL measurements were carried out with the samples mounted strain free in a helium-flow cryostat. The excitation source was the weakly focused 632.8 nm line of a He-Ne laser. The excitation intensity was kept well below the saturation threshold of the QDs. The signal was analyzed with a spectrally calibrated, nitrogen-purged Fourier-transform spectrometer using a liquid-nitrogen-cooled InSb detector. The PLE was excited with the monochromatized light of a 150 W tungsten lamp. The PL was then analyzed with a 0.5 m double-grating spectrometer and detected with a liquid-nitrogen-cooled InGaAs photodetector array sensitive up to 2 μm.

III. RESULTS

Figure 1 shows the low-temperature PL and PLE spectra of the samples. The emission of sample A comprises five peaks while that of sample B comprises nine peaks. The energy position of peak B1* encompasses those of peaks A1

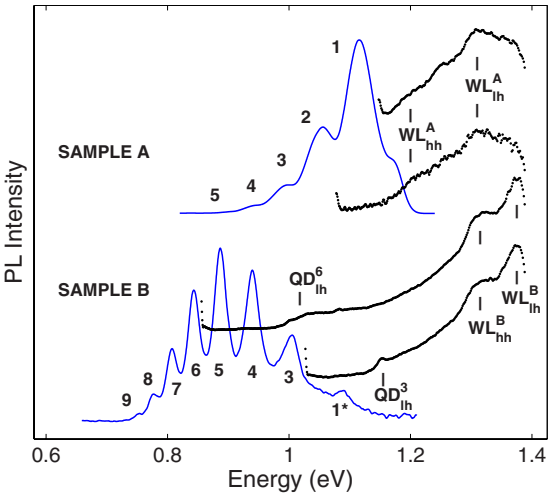

FIG. 1. (Color online) Low-temperature PL and PLE spectra of samples A and B. QD_{lh}, WL_{hh}, WL_{lh}, and InP refer to excitonic heavy- and light-hole resonances in QDs, WL, and the InP matrix, respectively.

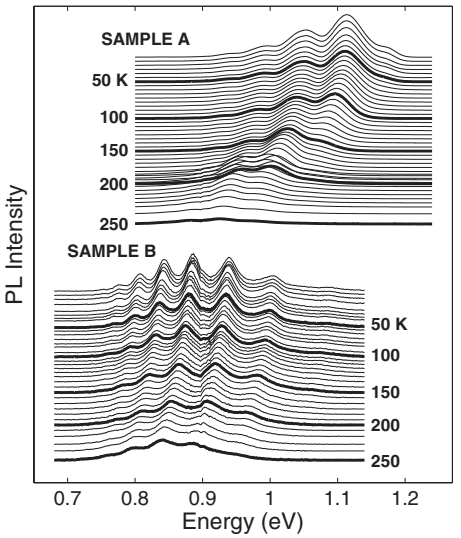

FIG. 2. Evolution of the PL spectra of samples A and B as a function of temperature.

and A2 while the positions of peaks B3–B5 are close to those of peaks A3–A5.

The PLE spectra of peaks A1 and A2 are similar to what was previously reported in thin InAs QWs.[27,30] They show an edge at 1.19 ± 0.01 eV and a resonance at 1.31 ± 0.01 eV that correspond, respectively, to the electron to heavy- and light-hole transitions in a 2-ML-thick InAs/InP QW as calculated with the tight-binding method.[27,31] It follows that the high-energy tail of the emission from sample A at low temperature corresponds to residual emission from the WL.

The PLE spectra of peaks B3 and B6 are also shown in Fig. 1. Two low-energy edges are observed, respectively, 150 meV (B3) and 170 meV (B6) above the emission peaks. They correspond to the first excited state QD_{lh}. Two other resonances appear at the same energies of 1.30 ± 0.01 eV and 1.37 ± 0.01 eV in both spectra. These are close to the expected transitions of a 1-ML InAs/InP QW. They can thus be attributed to the WL_{hh} and WL_{lh} transitions in sample B. We attribute the fact that the WL is thinner in sample B than in sample A to the longer interruption that took place during the growth of sample B. This probably allowed the formation of thicker QDs at the expense of the WL. The difference in energy of the fundamental WL optical transition is useful for our purpose as it adds another constraint to the thermal model described in Sec. IV.

The evolution of the PL spectra of both samples as a function of temperature is depicted in Fig. 2. The emission from peak A1 is rapidly quenched for $T > 100$ K while that of peak A2 remains nearly constant for $T < 170$ K. The intensity of peaks A3–A5 actually increases for $T \sim 200$ K before decreasing at higher temperatures. The emission from sample B is more robust as only peaks $B1^*$ and B3 show a significant intensity decrease at 300 K. No emission from QD excited states can be detected even at high temperatures.

IV. RATE-EQUATION MODEL

Our thermal model, which is schematized in Fig. 3, is similar to those developed in Refs. 4 and 6. A series of coupled steady-state rate equations that control the populations n_i in each state i is obtained from the detailed balance principle,[4]

$$-n_i\left(R_i + \sum_{j\neq i} N_j U_{ij}\right) + N_i \sum_{j\neq i} n_j U_{ji} + P_i = 0, \tag{3a}$$

where R_i is the recombination rate of state i, N_i the number of states per unit area, and U_{ij} the transfer cross section from state i to state j. P_i represents the carrier generation, ν_i is defined in Eq. (1) and

$$U_{ji} = U_{ij} \exp\left\{\nu_j \frac{(E_j - E_i)}{kT}\right\} \quad \text{if } E_j < E_i. \tag{3b}$$

We improved on previous models by incorporating several unique features. (i) Transfer from QDs to WL, from QDs to the InP matrix, and from WL to the InP matrix are allowed. (ii) The allowed states of the WL and the InP matrix

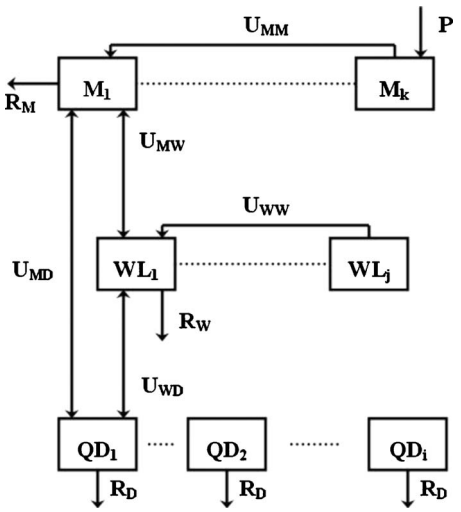

FIG. 3. Schematic of the coupled rate-equation model.

are distributed over a wide range of energy above their fundamental edge, E_g^W for the WL and E_g^M for InP. To make this fact numerically tractable, the WL is separated into segments of width ΔE_W extending from E_g^W to E_g^M. The effective number of states per unit area of each segment is $N_W = D_W \Delta E_W$, where $D_W = m_X^{\mathrm{InAs}}/\pi\hbar^2$ is the two-dimensional density of states in the WL. The InP matrix is similarly segmented. We assume a $\sqrt{E-E_g}$ dependence for its three-dimensional density of states. The number of states per unit area for a segment that extends from $E_i^{\min}$ to $E_i^{\min}+\Delta E_M$ is thus

$$N_{Mi} = \frac{2}{3} D_M \ell_M [(E_i^{\min} + \Delta E_M - E_g^M)^{3/2} - (E_i^{\min} - E_g^M)^{3/2}], \tag{4}$$

where $D_M = 2^{1/2}(m_X^{InP})^{3/2}/(\pi^2\hbar^3)$ (Ref. 32) and ℓ_M is the active thickness of the matrix.

(iii) $E_g^W(T)$ and $E_g^M(T)$ are assumed to follow the Varshni temperature dependence with the parameters of bulk InAs and InP, respectively.[33]

In order to restrain the number of adjustable parameters, the following assumptions were made:

$$R_i = \begin{cases} R_D & \text{if } i \in D, \\ R_W & \text{for } W \text{ lowest energy segment}, \\ R_M & \text{for } M \text{ lowest energy segment}, \\ 0 & \text{for all other states}, \end{cases} \tag{5a}$$

$$\nu_i = \begin{cases} \nu_D & \text{if } i \in D, \\ 1 & \text{if } i \in W, \end{cases} \tag{5b}$$

$$P_i = \begin{cases} P & \text{if } i = M \text{ highest energy segment}, \\ 0 & \text{if not}, \end{cases} \tag{5c}$$

$$U_{ij} = \begin{cases} 0 & \text{if } i \text{ and } j \in D, \\ U_{WD} & \text{if } i \in W \text{ and } j \in D, \\ U_{MD} & \text{if } i \in M \text{ and } j \in D, \\ U_{MW} & \text{if } i \in M \text{ and } j \in W, \\ U_{WW} & \text{if } i \text{ and } j \in W, \\ U_{MM} & \text{if } i \text{ and } j \in M, \end{cases} \tag{5d}$$

where D, W, and M refer, respectively, to the ensemble of QD, WL, and InP matrix states. We further assumed that the parameters in Eqs. (5) are independent of temperature.

In Eq. (5a), R_D corresponds to the QD radiative rate. As no emission from the WL nor the InP matrix is observed at high temperature, R_W and R_M correspond to nonradiative rates. R_W was assigned only to the lowest-energy segment because, in a QW, free excitons form two-dimensional polaritons that do not couple to photonlike polaritons propagating perpendicular to the QW plane unless their energy is within a small bandwidth near the bottom of the band.[34] Excitons must thus relax to the bottom of their energy band before they can recombine radiatively or nonradiatively.[35] A similar argument can be made for R_M.[36]

QD excited states are sometimes reported in the high-temperature PL from InAs/GaAs QDs.[5,14] In such a case, they should be included in the thermal model within an appropriate formalism. In our case however, no excited state emission is detected. Further, the energy difference between QD first excited state and ground state is higher than 150 meV, about twice as much than what is observed in typical InAs/GaAs QDs.[5] Thus, for our samples, the excited state population remains small at all temperatures and their effect on thermal quenching can be neglected.

V. DISCUSSION

To compare the simulations with the experiments, the data were treated as follows. The peak energy and integrated intensity of each peak at a given temperature was obtained by fitting the PL spectrum with a series of Gaussian peaks. This procedure was found to reproduce well the PL spectra except for peak B1*. Its peak energy and intensity was obtained by subtracting the intensity of all the other peaks from the total intensity of the PL emission. The energy position of each family of QDs served as input to the model.

In the model, the total number of QD states per unit area N_D and the QD recombination rate R_D are scaling factors. The relative number of states for each QD family was assumed to be given by the relative intensity of the PL at low temperature. ΔE_W and ΔE_M were set at 10 meV, a value close to the spectral extent of the WL and InP matrix absorption edges. In Eq. (5d), the parameters U_{WW} and U_{MM} were set to a high value to ensure that the excitons in the WL and the InP matrix are in thermal equilibrium. Finally, we fixed ℓ_M at 100 nm, a value close to the penetration length of the excitation source.[37] The model is thus left with seven adjustable materials parameters: R_W/R_D, R_M/R_D, $U_{WD}N_D/R_D$, $U_{MD}N_D/R_D$, U_{MW}, ν_D, and $E_g^W(0)$.

The result of our simulations is presented in Fig. 4 and the optimized parameters are listed in Table I. The uncertainties Δa_i of the optimized parameters were estimated using[38]

$$\Delta a_i = \left(\frac{1}{2}\frac{\partial^2 \chi^2}{\partial^2 a_i}\right)^{-1/2}. \tag{6}$$

Strictly speaking, Eq. (6) is only valid if the cross-partial derivatives $\partial\chi^2/\partial a_i \partial a_j$ are small with respect to the diagonal terms, which is not the case here. However, it gives a good estimate of the sensitivity of the fit to a given parameter.

The temperature dependence of all peaks from sample A are very well reproduced by our model. In particular, it reproduces the intensity increase in peaks A3–A5 when $T \gtrsim 180$ K. The fluctuations at high temperatures in the simulated curves are caused by the fluctuations in the energy positions of the QD families, which are inserted in the model for each temperature. The fitted value for $E_g^W(0)$ corresponds within uncertainties to the measured value of the low-energy edge WL_{hh} shown in Fig. 1. There is globally much less thermal quenching in sample B and thus less dynamics to constrain the model. To extract relevant information, we fixed $E_g^W(0)$ to the value of WL_{hh} obtained from the PLE spectra of sample B shown in Fig. 1. Here also, peaks B1*, B3, and B4 are well reproduced by our simulations. There was nearly no change in intensity for peaks B5–B9 while our model predicts a slight increase. The discrepancy can easily

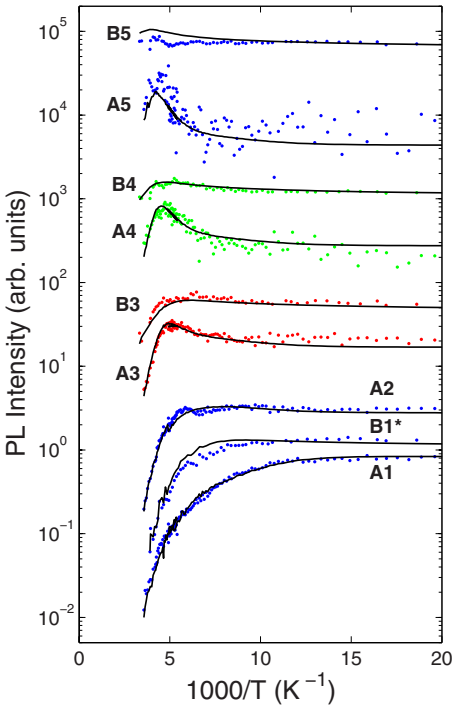

FIG. 4. (Color online) Arrhenius plot of the temperature dependence of the integrated intensity of the individual families of QD's. Labels A and B identify peaks from samples A and B, respectively. The curves have been shifted vertically for clarity.

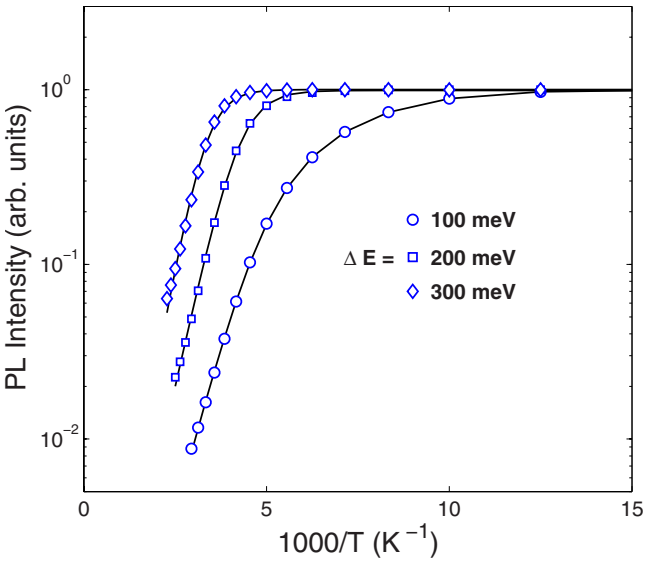

FIG. 5. (Color online) Arrhenius plot of the temperature dependence of the integrated intensity of simulated monomodal QD emission for three values of $\Delta E = E_g^W - E^D$. The solid lines are best fits using Eq. (2).

be explained by the neglect of the temperature dependence of the parameters of the model.

It can be seen from Table I that the parameters with high uncertainties are related to the InP matrix, an indication that for QDs, the main carrier escape and recapture channels are through the wetting layer. To further test this hypothesis, we deactivated the contribution to the thermal quenching of the InP matrix by fixing $R_M = 0$. To reduce further the number of adjustable parameters, $E_g^W(0)$ was fixed at the value of WL_{hh} for each sample. In the case of sample A, no significant change in the fits was detected when using the remaining set of five parameters. However, a further reduction in the number of parameters resulted in degraded fits. In particular, neither U_{MD} nor U_{MW} could be separately set to zero. Thus, our model requires that the carriers injected in the matrix be captured both by the dots and the WL. In the case of sample B, the matrix could be entirely removed from the model and the experimental data fitted with only three variable parameters. This shows that, for our samples, the thermal quenching occurs through carrier escape from QD to WL followed by a nonradiative recombination of the carriers in the WL.

As for the parameter ν_D, the simulations show that it is close to one half for our samples. As ν_D is the most critical parameter in our model, this indicates that electrons and holes escape from the QDs mostly as correlated *e-h* pairs. We thus corroborate the findings of Yang *et al.*[4] This is by no means a trivial result as there are no compelling reason for the escape mechanism to involve correlated *e-h* pairs rather than uncorrelated pairs or excitons.

It is instructive to simulate with our model the temperature dependence of the integrated intensity of a monomodal QD emission. We have generated a Gaussian distribution of 15 QD subfamilies centered at an energy E^D and shifted with respect to the WL by $\Delta E = E_g^W - E^D$. The FWHM of the distribution was fixed at $0.25\Delta E$, a value typical of monomodal InAs/GaAs QD emission.[7] We used in the simulations the same materials parameters as those found for sample A except for $\nu_D = 0.5$.

The result of our simulations for $\Delta E = 100$, 200, and 300 meV is shown as symbols in Fig. 5. The curves were analyzed with a sum of activated processes as described by Eq.

TABLE I. Parameters obtained by fitting the model to the experimental data. The numbers in parenthesis are the uncertainties Δa_i calculated with Eq. (6).

	R_W/R_D	R_M/R_D	ℓ_M (nm)	$U_{WD}N_D/R_D$	$U_{MD}N_D/R_D$	$U_{MW}N_W/R_D$	ν_D	$E_g^W(0)$ (eV)
Sample A (full set)	22 (1)	9 (18)	100[a]	12.3 (0.5)	5000 (300)	1800 (100)	0.64 (0.03)	1.19 (0.04)
Sample A (reduced set)	22 (1)	0[a]	100[a]	10.6 (0.5)	5000 (300)	1700 (100)	0.64 (0.03)	1.19[a]
Sample B (full set)	36 (2)	20 (10)	100[a]	51 (2)	20 (140)	9000 (9000)	0.51 (0.04)	1.30[a]
Sample B (reduced set)	36 (2)			44 (2)			0.49 (0.02)	1.30[a]

[a]Fixed parameter.

TABLE II. Parameters obtained by fitting the simulated data of Fig. 5 with Eq. (2).

ΔE (meV)	E_1^a (meV)	E_2^a (meV)
100	160	50
200[a]	190	
300[a]	230	

[a]Only one activation energy required.

(2). All curves are well reproduced with the activation energies given in Table II. The rapid drop of intensity at elevated temperatures is controlled by E_1^a. In all three cases, we find $E_1^a > \nu\Delta E$. Further, E_1^a does not correspond to any difference between the energy levels present in the model.

These simulations show that the difference between E_1^a and the activation energies inserted in the model comes from carrier transport in the WL and recapture by QDs. This induces a redistribution of the carriers within the subfamilies that slows down thermal quenching, resulting in an ensemble effective activation energy higher than actual ones. Therefore, in systems where recapture competes with recombination, Eq. (2) gives empirical activation energies that might not correspond to any physical process at play.

VI. CONCLUSIONS

We have developed a system of coupled rate equations for the temperature dependence of the multimodal PL of InAs/InP QDs. The model includes carrier escape to the InAs wetting layer and to the surrounding InP matrix as well as carrier transport and recapture. Even though our model comprises seven adjustable parameters, the constraints imposed by the simulation of the complex temperature behavior of up to five different QD families makes our fits robust. We find that thermal quenching is induced by carrier escape to the wetting layer followed by nonradiative recombination. Further, our results clearly establish that, for both samples examined, the escape activation energies are close to one half that of the optical gap between the wetting layer and the QDs. This indicates that electrons and holes are emitted as correlated pairs rather than excitons. Finally, we show that carrier redistribution within the QD energy levels as temperature is increased can yield activation energies obtained from analyzing PL integrated intensities that do not correspond to any actual physical process.

We cannot assert whether correlated-pair escape is characteristic of self-assembled QDs or specific to the InAs/InP system. The latter case could mean that the temperature dependence of QD optical emission is governed not only by confinement energy but also by microscopic parameters such as the size and shape of individual QDs. A better theoretical understanding of the interactions between QDs and their environment is thus not only of great fundamental interest but could also impact the design of QD-based devices.

ACKNOWLEDGMENTS

This work was supported by the Natural Sciences and Engineering Research Council of Canada (NSERC) and the Fonds Québécois de la Recherche sur la Nature et les Technologies (FQRNT).

*richard.leonelli@umontreal.ca

[1] D. Bimberg, M. Grundman, and N. N. Ledentsov, *Quantum Dot Heterostructures* (Wiley, New York, 2001).
[2] *Nano-Optoelectronics: Concepts, Physics and Devices*, edited by M. Grundmann (Springer, Berlin, 2002).
[3] D. Kim, S. E. Economou, S. C. Badescu, M. Scheibner, A. S. Bracker, M. Bashkansky, T. L. Reinecke, and D. Gammon, Phys. Rev. Lett. **101**, 236804 (2008).
[4] W. D. Yang, R. R. Lowe-Webb, H. Lee, and P. C. Sercel, Phys. Rev. B **56**, 13314 (1997).
[5] R. Heitz, I. Mukhametzhanov, A. Madhukar, A. Hoffmann, and D. Bimberg, J. Electron. Mater. **28**, 520 (1999).
[6] S. Sanguinetti, M. Henini, M. Grassi Alessi, M. Capizzi, P. Frigeri, and S. Franchi, Phys. Rev. B **60**, 8276 (1999).
[7] E. C. Le Ru, J. Fack, and R. Murray, Phys. Rev. B **67**, 245318 (2003).
[8] K. Akiba, N. Yamamoto, V. Grillo, A. Genseki, and Y. Watanabe, Phys. Rev. B **70**, 165322 (2004).
[9] P. Dawson, O. Rubel, S. D. Baranovskii, K. Pierz, P. Thomas, and E. O. Gobel, Phys. Rev. B **72**, 235301 (2005).
[10] S. Sanguinetti, D. Colombo, M. Guzzi, E. Grilli, M. Gurioli, L. Seravalli, P. Frigeri, and S. Franchi, Phys. Rev. B **74**, 205302 (2006).
[11] P. Dawson, E. O. Göbel, K. Pierz, O. Rubel, S. D. Baranovskii, and P. Thomas, Phys. Status Solidi B **244**, 2803 (2007).
[12] T. V. Torchynska, J. L. C. Espinola, L. V. Borkovska, S. Ostapenko, M. Dybiec, O. Polupan, N. O. Korsunska, A. Stintz, P. G. Eliseev, and K. J. Malloy, J. Appl. Phys. **101**, 024323 (2007).
[13] A. Chahboun, M. I. Vasilevskiy, N. V. Baidus, A. Cavaco, N. A. Sobolev, M. C. Carmo, E. Alves, and B. N. Zvonkov, J. Appl. Phys. **103**, 083548 (2008).
[14] T. V. Torchynska, J. Appl. Phys. **104**, 074315 (2008).
[15] W.-M. Schulz, R. Roßbach, M. Reischle, G. J. Beirne, M. Bommer, M. Jetter, and P. Michler, Phys. Rev. B **79**, 035329 (2009).
[16] L. Seravalli, G. Trevisi, P. Frigeri, S. Franchi, M. Geddo, and G. Guizzetti, Nanotechnology **20**, 275703 (2009).
[17] M. Grundmann and D. Bimberg, Phys. Rev. B **55**, 9740 (1997).
[18] R. Heitz, A. Kalburge, Q. Xie, M. Grundmann, P. Chen, A. Hoffmann, A. Madhukar, and D. Bimberg, Phys. Rev. B **57**, 9050 (1998).
[19] P. Buckle, P. Dawson, S. Hall, X. Chen, M. Steer, D. Mowbray, M. Skolnick, and M. Hopkinson, J. Appl. Phys. **86**, 2555 (1999).
[20] M. Abbarchi, C. Mastrandrea, T. Kuroda, T. Mano, A. Vinattieri, K. Sakoda, and M. Gurioli, J. Appl. Phys. **106**, 053504 (2009).
[21] H. Folliot, S. Loualiche, B. Lambert, V. Drouot, and A. Le

Corre, Phys. Rev. B **58**, 10700 (1998).
[22] P. J. Poole, J. McCaffrey, R. L. Williams, J. Lefebvre, and D. Chithrani, J. Vac. Sci. Technol. B **19**, 1467 (2001).
[23] S. Raymond, S. Studenikin, S. J. Cheng, M. Pioro-Ladriere, M. Ciorga, P. J. Poole, and M. D. Robertson, Semicond. Sci. Technol. **18**, 385 (2003).
[24] M. D. Robertson, J. C. Bennett, A. M. Webb, J. M. Corbett, S. Raymond, and P. J. Poole, Ultramicroscopy **103**, 205 (2005).
[25] Y. Sakuma, M. Takeguchi, K. Takemoto, S. Hirose, T. Usuki, and N. Yokoyama, J. Vac. Sci. Technol. B **23**, 1741 (2005).
[26] A. Michon, I. Sagnes, G. Patriarche, G. Beaudoin, M. N. Mérat-Combes, and G. Saint-Girons, J. Appl. Phys. **100**, 033508 (2006).
[27] A. Lanacer, N. Shtinkov, P. Desjardins, R. A. Masut, and R. Leonelli, Semicond. Sci. Technol. **22**, 1282 (2007).
[28] C. Dion, P. Desjardins, N. Shtinkov, M. D. Robertson, F. Schiettekatte, P. J. Poole, and S. Raymond, Phys. Rev. B **77**, 075338 (2008).
[29] D. Frankland, R. A. Masut, and R. Leonelli, J. Vac. Sci. Technol. A **20**, 1132 (2002).
[30] P. Paki, R. Leonelli, L. Isnard, and R. A. Masut, Appl. Phys. Lett. **74**, 1445 (1999).
[31] N. Shtinkov, P. Desjardins, and R. A. Masut, Phys. Rev. B **66**, 195303 (2002).
[32] P. Y. Yu and M. Cardona, *Fundamentals of Semiconductors* (Springer, Berlin, 2004).
[33] O. Madelung, *Semiconductors: Data Handbook*, 3rd ed. (Springer, Berlin, 2004).
[34] T. C. Damen, J. Shah, D. Y. Oberli, D. S. Chemla, J. E. Cunningham, and J. M. Kuo, Phys. Rev. B **42**, 7434 (1990).
[35] R. Leonelli, C. A. Tran, J. L. Brebner, J. T. Graham, R. Tabti, R. A. Masut, and S. Charbonneau, Phys. Rev. B **48**, 11135 (1993).
[36] T. Steiner, M. L. W. Thewalt, E. S. Koteles, and J. P. Salerno, Phys. Rev. B **34**, 1006 (1986).
[37] Simulations were also run with ℓ_M as an adjustable parameter without any significant difference.
[38] P. R. Bevington and D. K. Robinson, *Data Reduction and Error Analysis for the Physical Sciences*, 3rd ed. (McGraw-Hill, Boston, 2003).